condensed matter

MDPI

Article

Surface Excitations, Shape Deformation, and the Long-Time Behavior in a Stirred Bose–Einstein Condensate

Qing-Li Zhu [1,2] and Jin An [1,3,*]

1 Department of Physics, National Laboratory of Solid State Microstructures, Nanjing University, Nanjing 210093, China; zhuqingli218@163.com
2 Department of Information Engineering, Nanjing Normal University Taizhou College, 225300 Taizhou, China
3 Collaborative Innovation Center of Advanced Microstructures, Nanjing University, Nanjing 210093, China
* Correspondence: anjin@nju.edu.cn

Received: 10 September 2018; Accepted: 23 November 2018; Published: 25 November 2018

Abstract: The surface excitations, shape deformation, and the formation of persistent current for a Gaussian obstacle potential rotating in a highly oblate Bose–Einstein condensate (BEC) are investigated. A vortex dipole can be produced and trapped in the center of the stirrer even for the slow motion of the stirring beam. When the angular velocity of the obstacle is above some critical value, the condensate shape can be deformed remarkably at the corresponding rotation frequency followed by surface wave excitations. After a long enough time, a small number of vortices are found to be either trapped in the condensate or pinned by the obstacle, and a vortex dipole or several vortices can be trapped at the beam center, which provides another way to manipulate the vortex.

Keywords: Bose–Einstein condensates; surface excitations; vortex dipoles; superfluid flow

1. Introduction

Quantized vortex is a topological singularity in a superfluid or superconductor, where the phase of the order parameter varies by an integer multiplying 2π when following a closed path around the defect. Due to its topological nature and the conservation of circulation, a vortex can be eliminated only by annihilation with an antivortex or moving to the boundary of the system [1].

Atomic Bose–Einstein condensate (BEC) provides a very convenient platform to investigate the characteristics of quantum vortices due to their experimental versatility [2–6]. Besides the studies of static vortices in the rapidly rotating trap, optical lattices, and dipolar BECs [7–14], there has been an increasing interest in the dynamical properties of vortices such as vortex nucleation [15–18] and evolution [19–24]. In addition, much work has been done on the vortex structure in multi-component [25,26] and spinor BECs [27–29], as well as the collisions and evolution of vortex loops and knots in three-dimensional BECs [30–37].

One of the important developments in atomic BEC is the recent experimental observations of a vortex dipole when a repulsive Gaussian obstacle moves through a pancake-shaped condensate [38,39]. Subsequently, much theoretical and experimental effort has been directed toward the topic of vortex dipoles. The studies mainly focus on the vortex shedding mechanism [40–43], topological excitation [42,44], and persistent current [45]. Additionally, vortex dipoles induced in oscillating potential [46], at finite temperatures [47], and under spin-orbit coupling [48] have been extensively studied. The experimental technique using two blue-detuned laser beams as "tweezers" provides realistic possibilities to pin and manipulate vortices [49–51]. Recent progress in a toroidal geometry [52–58] has opened a new prospect to study the superfluidity and vortex excitation using a rotating barrier or weak link [53,59,60]. When a weak link rotates in an annular BEC, it is found that surface modes can be excited, and the vortex can come into the condensate from the outside [57]. Furthermore, a persistent flow in a toroidal trap can be created by stirring with a rotating barrier [54]. For a highly oblate BEC stirred by a laser beam, studies have been done on the shape deformation elliptically and triangularly [61,62]. However, there is a lack of extensive study on this topic, and, more importantly, there have been no investigations on shape deformation for larger angular momentum, such as when the quantum number is 6 and 7. Moreover, the vortex dipoles inside the obstacle on their nucleation, the splitting properties, and the long-time dynamical behavior is less concerned and studied but is of great interest.

In this paper, by solving the time-dependent damped Gross–Pitaevskii (GP) equations, we reveal the shape deformation and long-time dynamical behaviors of a highly oblate BEC stirred by a rotating laser beam. The shape of the condensate deformed heavily due to excitations of many surface waves with relatively lower angular momenta. After a long enough time, a small numbers of vortices can be left either trapped in the condensate or pinned by the obstacle. On the other hand, stirring BEC by a rotating blue-detuned laser beam can cause a vortex dipole or several vortices to be pined at the beam center.

2. Model

Consider a single-component BEC described by the normalized macroscopic wave function $\psi(\mathbf{r},t)$. In the mean-field framework, the dynamics of a system with N weakly interacting identical atoms close to thermodynamic equilibrium and being subjected to weak dissipation can be described by the damped GP equation [63]:

$$(i-\gamma)\hbar\partial_t\psi = [\frac{-\hbar^2\nabla^2}{2m} + V(\mathbf{r}) + Ng|\psi|^2)]\psi \tag{1}$$

where $V(\mathbf{r}) = \frac{1}{2}m(\omega_t^2x^2 + \omega_t^2y^2 + \omega_z^2z^2)$ is the axially symmetric harmonic trap potential, and ω_t, ω_z are the radial and axial trap frequencies. The parameter γ in the GP equation is a dimensionless, phenomenological, damping constant. It takes into account the quantum and thermal fluctuations from the background and is introduced to fit the experiment. In studies of vortex excitations in an annular BEC [56], γ is chosen to be 0.0015, by which the measured lifetime of the vortices is consistent with the experimental result in [54]. The damped GP equation has been extensively employed to study the dynamics of systems in the presence of thermally induced dissipation [24,50,51,56,57].

We focus in this paper on a highly oblate BEC with $\omega_z \gg \omega_t$. In this extreme limit, the axial dimension is tightly suppressed that the motion along the z direction can be neglected and atoms can move only within the $x-y$ plane. The normalized ψ can thus be written as $\psi(\mathbf{r},t) = \psi_{2D}(x,y,t)\phi_0(z)$, where $\phi_0(z) = (\pi a_z^2)^{-1/4}e^{-z^2/2a_z^2}$ is the ground state for the potential $V_z(z)$, with $a_z = \sqrt{\hbar/m\omega_z}$ the characteristic length of the vertical harmonic oscillator. The atom–atom contact interaction is $g = 4\pi\hbar^2 a_s/m$, with a_s as the s-wave scattering length. In the numerical computations, we discretize the $x-y$ plane into a square lattice with $x(i) = ia$ and $y(j) = ja$. The artificial lattice constant a must be much less than the characteristic length $l = \sqrt{\hbar/m\omega_t}$ of the axial harmonic oscillator to validate the simulations [64]. Furthermore, a should also satisfy the condition of $a \ll \xi$, with ξ as the condensate healing length. For the time evolution, the fourth-order Runge–Kutta method is employed at each time step. The central-difference formula is used mainly to calculate the kinetic term. Introducing dimensionless $\psi(i,j)$, by substituting $\psi(\mathbf{r})$ with $\frac{1}{\sqrt{a^2a_z}}\psi(i,j)$, we thus obtain the following lattice-version GP equations:

$$\begin{aligned}(i-\gamma)\hbar\partial_t\psi(i,j) =& \{-t_0[\psi(i-1,j)+\psi(i+1,j)+\psi(i,j-1)+\psi(i,j+1)-4\psi(i,j)] \\ &+ [\tilde{V}(i^2+j^2) + N\tilde{g}|\psi(i,j)|^2]\psi(i,j)\}\end{aligned} \tag{2}$$

where $t_0 = \frac{\hbar^2}{2ma^2}$, $\tilde{V} = \frac{1}{2}m\omega_t^2 a^2$, and $\tilde{g} = \frac{4\pi a_s \hbar^2}{ma^2 a_z}$. Since all the parameters t_0, $\tilde{V}$, $\tilde{g}$, and $\hbar/t$ have the scale of energy, it is convenient to introduce dimensionless parameters $V' = V/t_0$, $g' = g/t_0$, and $t' = t/(\hbar/t_0)$, measured in units of t_0. All of these parameters are actually only dependent of a/l and a_s/a_z. A straightforward analysis leads to the following expressions of $V' = (\frac{a}{l})^4$ and $g' = 8\pi\frac{a_s}{a_z}$. Note that g' is essentially independent of the artificial lattice constant a.

We assume the system consists of ^{87}Rb atoms. Thus, we have $m \approx 87m_p$, with m_p as the mass of proton. We choose the trap frequency $\omega_t = 2\pi \times 10$ Hz. l is then estimated to be about 3.4 µm. When the square lattice we study takes a typical size of 200×200 and $(a/l)^2$ is chosen to be 0.008, the system has a size of about 60 µm × 60 µm and $\hbar\omega_t/t_0 = 2(a/l)^2 = 0.016$, $\hbar/t_0 = 0.2$ ms, and $V' = 0.000064$. In addition, to guarantee both the convergence and efficiency of iteration of the GP equations, dt' is chosen to be between 10^{-4} and 10^{-2} in numerical calculations. We control the convergence from the density distribution until the precision reaches the level of 10^{-10} in each mesh.

3. Results and Discussions

When a blue-detuned laser beam is rotating uniformly with angular velocity Ω in BEC, the obstacle produced by it can be well described as a moving Gaussian potential:

$$V_{GOP}(x,y) = V_0 e^{-\frac{1}{\sigma^2}\{[x-x_0(t)]^2+[y-y_0(t)]^2\}} \tag{3}$$

where $\{x_0(t), y_0(t)\} = \{R\cos(\Omega t), R\sin(\Omega t)\}$, with R as the distance between the obstacle and trap center, and σ and V_0 are the laser beam waist and barrier height of the potential, respectively. The detailed behavior of the stirred BEC depends sensitively on σ/ξ and V_0 [41–43,49,53,65], and in the following they are fixed to be $V_0 = 8t_0$, $\sigma = 3.5\xi$. In such a quasi-2D atomic system, at the trap center, the chemical potential μ is estimated to be $\mu = n_0 g \approx 0.5t_0$, where n_0 is the atomic density $|\psi(i,j)|^2$. Therefore, the condensate healing length $\xi = \frac{\hbar}{\sqrt{2m\mu}}$ and the sound velocity $v_s = \sqrt{\frac{\mu}{m}}$ are on the order of $0.2l$ and 1.15 mm/s, respectively. By starting from the ground state of the BEC in the presence of a static obstacle, the uncontrollable excitations are prevented from an abrupt motion of the obstacle. Before the obstacle moves with a constant angular velocity Ω, the angular velocity is assumed to increase linearly with time from zero until reaching Ω. In the following, γ is set to be 1.5×10^{-3}. We find our results do not depend qualitatively on the specific value of γ when it is in the range of 0.001–0.005.

According to the Landau criterion, a superfluid becomes dissipative when it flows above a certain critical velocity v_c via generating its elementary excitations such as phonons and vortices. For a homogeneous system, the Landau critical velocity is equal to the speed of sound v_s [66]. The critical velocity is believed to provide an upper bound for a moving hard cylinder in a uniform BEC and depends on the barrier height V_0 and width σ in a harmonic tap [41]. Here, the critical velocity v_c is defined as the value of the obstacle velocity $v = R\Omega$, at which the vortex excitation begins to be generated into the BEC by the obstacle and depends on the distance R from the BEC center. However, even when v is much smaller than v_c, a vortex dipole can be produced and tightly trapped by the obstacle. Since the obstacle potential is finite in spite of being large, the local density n of the BEC within the small space occupied by the obstacle is rather small but finite. The small local density thus lowers the speed of sound locally, leading to the local excitations within the obstacle according to the Landau criterion. When the obstacle velocity v is below v_c but not too small, the vortex dipole direction can be identified from the phase profile of the BEC, which rotates uniformly within the obstacle but always remains perpendicular to the motion direction of the obstacle, as exhibited in Figure 1.

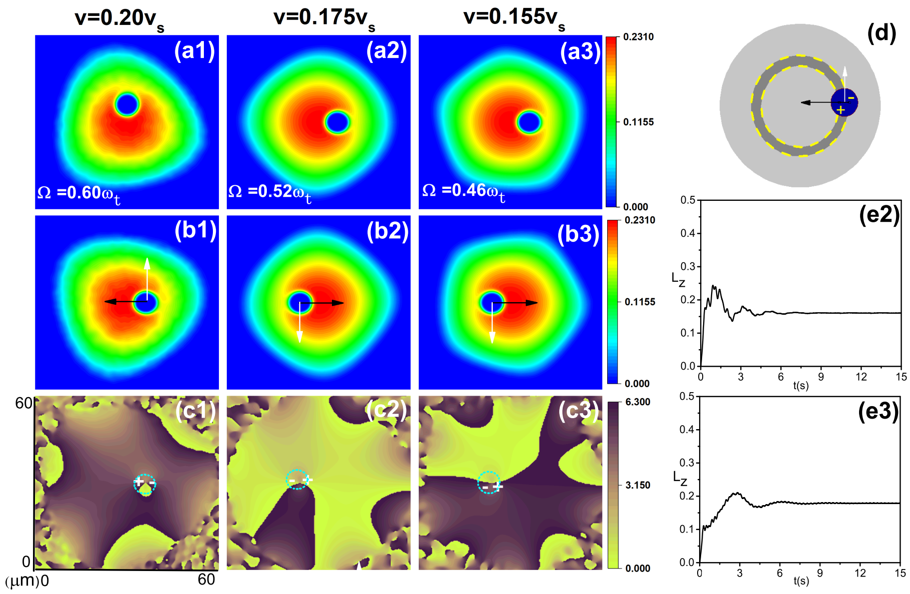

Figure 1. The left panels denote the density and phase profiles when the obstacle velocity is below the critical value, where the generated vortex–antivortex pair has not been split out. The upper two rows show the evolution of the density distribution at two instants. The figures in the bottom row (**c1**)–(**c3**) show the phase corresponding to (**b1**)–(**b3**). Here, $Ng' = 5000$. The "+" and "−" signs denote the vortex and antivortex of the pair. The white and black arrows show the directions of obstacle motion and vortex dipole, which are always perpendicular to each other. The green dotted circles in (**c1**)–(**c3**) show the boundary of the obstacle. The angular momenta per atom $\overline{L}_z = -i\hbar \int d\mathbf{r}\psi^*(\mathbf{r})(x\partial y - y\partial x)\psi(\mathbf{r})$ as functions of time for (**b2**) and (**b3**) are exhibited accordingly in (**e2**) and (**e3**). The angular momentum contribution from the vortex dipole is schematically shown in (**d**), where only the atoms in the dark shaded annular region effectively contribute to L_z, $\hbar$ per atom.

Besides the critical velocity v_c, there exists a critical angular velocity $\Omega_c = \min\{\omega_l/l\}$ according to an analog of the Landau criterion [67–69], where ω_l is the surface-wave excitation energy. For smaller l, by solving the hydrodynamic equations of a superfluid, one can obtain the general dispersion law $\omega_l = \sqrt{l}\omega_t$ [70]. For the parameters chosen, Ω_c is estimated to be about $0.3\omega_t$, above which surface waves can be excited. However, the surface excitations with larger l can hardly be identified from the density or phase profiles of the BEC obtained numerically. On the other hand, for smaller l, $\omega_l/l = \omega_t/\sqrt{l}$ can also be viewed as the minimum excitation frequency for generating a surface excitation with angular momentum l, indicating that the surface excitations with smaller l can be possibly found upon increasing Ω up to a sufficient large value. It is found in our calculations that, when $\Omega = 0.6\omega_t$, the density of the BEC is deformed triangularly. Figure 1(a2)–(a3) also show the similar behavior of the condensate when the rotating frequency Ω is slightly larger than $\omega_t/2(\omega_t/\sqrt{5})$, where the condensate is deformed tetragonally(pentagonally). Furthermore, by investigating the time evolution of density, we find that the shape deformation of the condensate is rotating rigidly nearly at the same angular velocity as the obstacle, as can be seen in Figure 1, where the two density profiles in each column show the evolution of the density at two instants. This feature can be explained as follows. The condensate can be viewed to be composed of two parts: the surface and core parts. The surface part with strong shape deformation consists of atoms which carry the surface excitations and their angular momenta, while the core part is left nearly motionless. The surface excitations with angular momentum l produce a density deviation $\delta n \propto e^{i(l\theta - \omega_l t)} = e^{il(\theta - \frac{\omega_l}{l}t)}$, indicating that the corresponding shape deformation is rotating with an angular velocity ω_l/l, while the rotating obstacle can be seen as a density perturbation $\delta n \propto \delta(\theta - \Omega t) = \sum \frac{1}{2\pi} e^{in(\theta - \Omega t)}$. The resonance occurs when Ω approximately equals ω_l/l, where many surface waves with angular momentum l are excited, leading to a heavy shape deformation in the form of an l-regular polygon. In this situation, the surface part is also rotating nearly synchronously with the obstacle.

On the other hand, the surface part is believed to contain much fewer atoms than the core part, so the average angular momentum per atom is approaching a relative small value (about 0.15 for the case in Figure 1(c2) in the long-time evolution). Notice that the contribution to angular momentum from the vortex dipole is expected to be quite small. As shown schematically in Figure 1d, the vortex dipole's contribution to the angular momentum is estimated to be $\sim \frac{d_0}{R_{TF}} \ll 0.1$ with d_0 the vortex–antivortex distance and R_{TF} the TF radius, since d_0 is found to be much less than the healing length ξ.

Since $R\omega_t/\sqrt{2} > v_c$ for $R = 1.8l$, the elliptical deformation due to $l = 2$ surface waves cannot be observed. However, for a smaller $R = 1.3l$, our calculations confirm the existence of the elliptically deformed BEC for $\Omega_0 = \omega_t/\sqrt{2}$, which is consistent with the experimental observations [5,67]. In Figure 2, we plot our results of the critical angular velocity for surface wave excitations when l varies from 2 to 8 and comparing them with the analytical value of $\omega_t/\sqrt{l}$.

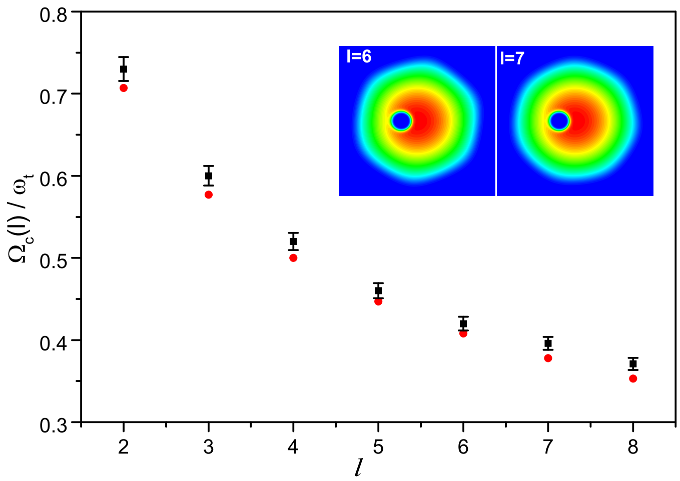

Figure 2. Critical frequency Ω for surface mode excitations as the surface wave angular momentum l changing from 2 to 8. The red circles are the analytical values by $\Omega = \omega_t/\sqrt{l}$. Each data point denoted by black square is fixed based on 10 measurements numerically, and the error bar indicates the standard deviation.

We now turn our attention to the critical velocity and mechanism of the vortex nucleation. When a circular cylinder is passing through a two-dimensional homogenous system, the critical velocity is calculated numerically and estimated to be $v_c = 0.37v_s$ in the large-cylinder limit $R \gg \xi$, with R as the radius of the cylinder [71]. Experimentally, the minimal measured value of v_c/v_s for vortex shedding in a highly oblate BEC reaches 0.1 [41]. In our model, when $R = 1.8l$, v_c is estimated to be $v_c = 0.21v_s\,|_{r=R} = 242\ \mu m/s$, at which the vortex dipole starts to split. This critical value can also be confirmed from the drag force defined by $F = i\hbar\partial_t \int d\mathbf{r}(\Psi^\dagger\nabla\Psi)$[17]. The drag forces along the x and y directions at $0.20v_s$ and $0.21v_s$ are illustrated in Figure 3. Under the same velocity, both x and y directions gradually exhibit periodic oscillations with the same frequency due to the periodic motion of obstacle. While at v_c the drag forces gradually decrease since the accumulated energy is released [72]. The antivortex starts to separate from the vortex and move toward the barrier edge, while the vortex is still pinned at the obstacle center, as schematically shown in Figure 4a. Meanwhile, a sharp corner of the density hole appears (Figure 4b), long before the antivortex leaves the barrier edge. The antivortex is then released from the obstacle and moves gradually to the boundary of the condensate. When v is slightly above $0.26v_s$, after the first antivortex escapes from the obstacle, another vortex–antivortex pair will be generated and subsequently the new antivortex starts to escape, leaving the two vortices trapped at the center by the obstacle (see Figure 4). When $v > 0.3v_s$, more vortex–antivortex pairs will be generated during the whole stirring process and more vortices can be trapped by the obstacle. It is interesting to compare the microscopic mechanism of vortex nucleation to the case of a weak link rotating in a torodial BEC. As was shown in [57], at a low rotation rate above the threshold value, a vortex enters the weak link from the outside and approaches the antivortex to create a vortex–antivortex pair, since the critical velocity for vortex nucleation is reached first at the outer edge of the condensate.

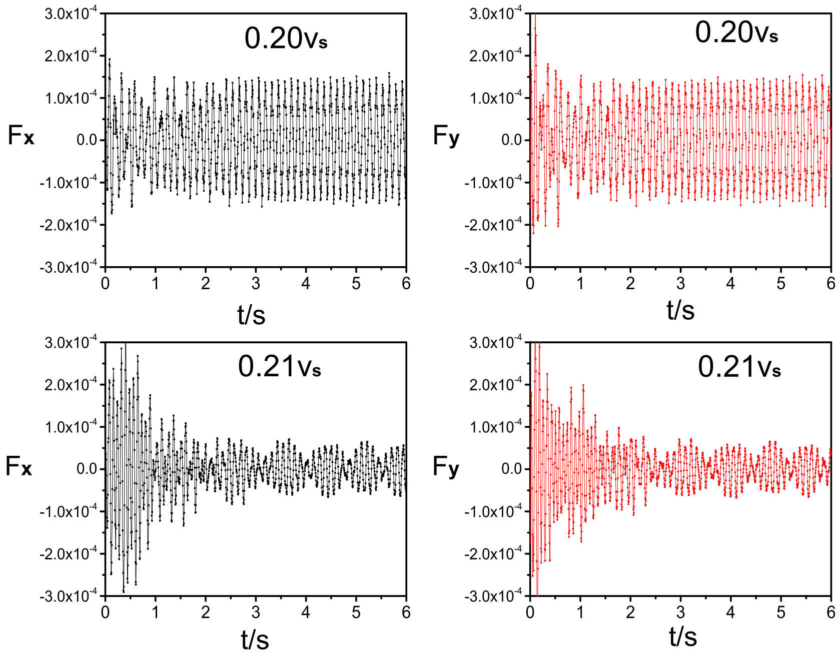

Figure 3. Time evolution of drag forces exerted on the GOP along the x and y directions colored with black and red solid lines, respectively. The velocity of the obstacle is $0.2v_s$ (top) and $0.21v_s$ (bottom). The parameter here is $R = 1.8l$.

After stirring for over 100 circles, the BEC reaches a metastable state, which shows nearly time-independent features. This means the obstacle will stop shedding vortices after a long-time stirring. This can be better understood in the limit of V_0 being infinite. The vortices trapped by the obstacle or the condensate have changed the distribution of the superfluid velocity around the obstacle. According to Landau criterion, no vortex will be excited, if all velocities are below the critical value, leading to the formation of persistent current after a long-time stirring. Now we study the long-time behavior of the BEC and focus on the vortex number left in the condensate. After a long enough time, all antivortices will leave the condensate, and only vortices are left. Among the remaining vortices, several are pinned by the obstacle, and the others are loosely trapped near the trap center. The nearly time-independent angular momentum also confirms the stability of the long-time behavior of the BEC. In the parameter region we studied, three vortices at most can be trapped by the obstacle. These results are demonstrated in Figure 5. The number of trapped vortices is summarized in Table 1. If the laser beam stops moving suddenly, the trapped vortices will be released, but finally one or two of them will be trapped at the obstacle center and stabilized to form persistent current state. When the laser beam is ramping off, the trapped vortices will become free and will then move to the boundary. Comparing with the method for vortex manipulation using the chopstick beams [50], the rotating obstacle in our model plays a key role in the mechanism of pinning vortices, which provides another way to manipulate a vortex. For the parameters we studied here, we only focus on the velocity regime $v < 1.7v_c$, since, when $v > 2v_c$, many vortices are generated quickly such that the stirred BEC is in a turbulent state. Within the regime $v_c < v < 1.7v_c$, it is not from the boundary but within the obstacle center in the form of a vortex pair that the vortices are created.

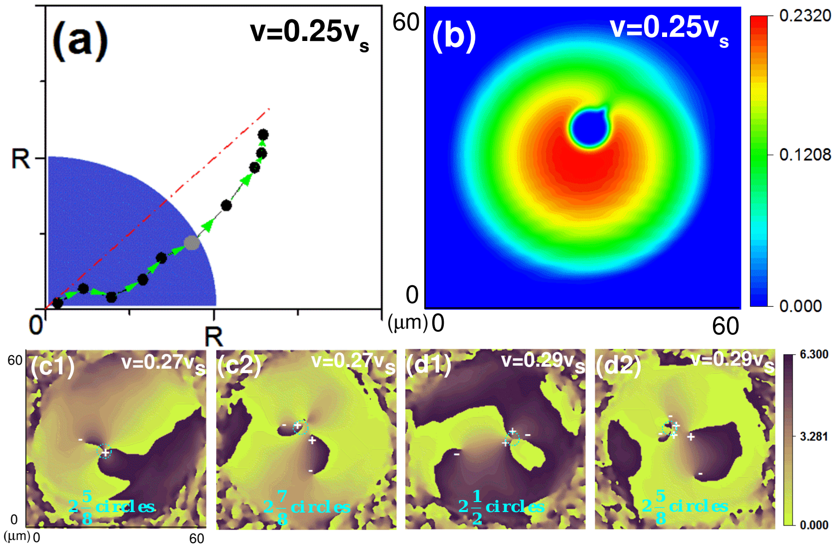

Figure 4. (**a**) The orbit of the antivortex of the vortex dipole in the frame of reference of the moving obstacle, when the obstacle velocity is slightly above the critical value. Here, the blue region represents the density hole of the obstacle with radius $\sigma = 3.5\xi$, where ξ is the healing length at the trap center. The red dash-dotted line denotes that between the centers of the obstacle and trap. The 10 circle dots are representative positions of antivortex as it is escaping from the obstacle within the first half circle of stirring, where the arrows indicate the motion directions of the antivortex; (**b**) The density profile of the BEC when the antivortex moves to the gray-shaded dot in (a), where the spike denotes the exact position where the antivortex leaves the obstacle. (**c1**,**d1**) and (**c2**,**d2**) are the phase profiles before and after the generation of the second (third) vortex dipole within one-fourth (eighth) of the circle of stirring when $v = 0.27v_s$ ($v = 0.29v_s$), where only two (three) vortex dipoles are generated in the whole stirring process.

Table 1. The number of trapped vortices after stirring BEC for a long time, for the parameters we studied. While n_1 denotes the number of trapped vortices within the obstacle, n_2 denotes that outside the obstacle. The total number is $n = n_1 + n_2$.

v	$R = 3.6l$			$R = 1.8l$		
	n_1	n_2	n	n_1	n_2	n
$1.00v_c$–$1.25v_c$	1	0	1	1	0	1
$1.25v_c$–$1.35v_c$	2	0	2	2	0	2
$1.35v_c$–$1.50v_c$	2	1	3	3	0	3
$1.50v_c$–$1.70v_c$	3	1	4	2	4	6

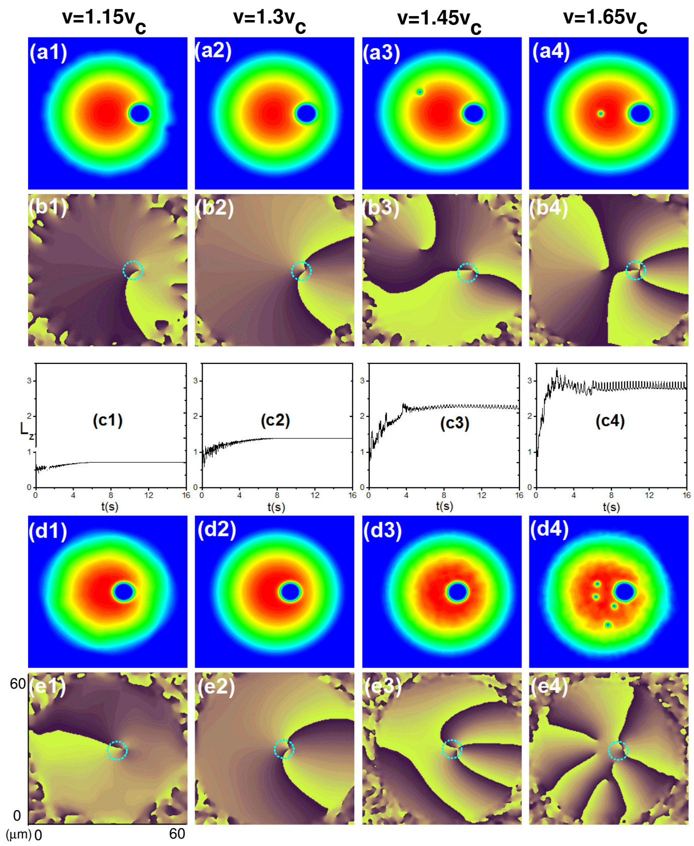

Figure 5. The long-time dynamical behavior of the condensate when the obstacle velocity is above the critical value v_c with $v_c = 255$ μm/s at $R = 3.6l$ and $v_c = 242$ μm/s at $R = 1.8l$, by stirring the BEC for over 100 circles. The upper (lower) two panels denote the density and phase profiles with $R = 3.6l$ ($R = 1.8l$). The middle panels denote the angular momenta per atom corresponding to the cases from (**a1**) to (**a4**), respectively.

4. Conclusions

We have performed numerical calculations of the quasi-two-dimensional GP equation to investigate the surface wave excitations and the long-time behavior of vortices in a stirred, highly oblate condensate. Surface waves can be excited with the condensate shape being deformed heavily at the corresponding rotation frequency. A vortex–antivortex pair can be created in the obstacle center even when the obstacle velocity is relatively small. Once the obstacle velocity reaches a critical value, the antivortex starts to separate from the vortex and then leaves the obstacle regime. Furthermore, after a long enough time, a small number of vortices are found to be left either trapped in the condensate or pinned by the obstacle, and the number of them depends on the velocity and position of the obstacle.

Author Contributions: Conceptualization: Q.-L.Z. and J.A.; Methodology: J.A.; Validation, Q.-L.Z. and J.A.; Formal Analysis: J.A.; Investigation: Q.-L.Z.; Resources: J.A.; Data Curation: Q.-L.Z.; Writing original Draft Preparation: Q.-L.Z.; Writing review & Editing: J.A.; Supervision: J.A.; Funding Acquisition, J.A.

Funding: This research was funded by the NSFC Project No.11874202 and 973 Projects No.2015CB921202.

Conflicts of Interest: The authors declare no conflict of interest.

References

1. Soskin, M.S.; Gorshkov, V.N.; Vasnetsov, M.V.; Malos, J.T.; Heckenberg, N.R. Topological charge and angular momentum of light beams carrying optical vortices. *Phys. Rev. A* **1997**, *56*, 4064. [CrossRef]

2. Matthews, M.R.; Anderson, B.P.; Haljan, P.C.; Hall, D.S.; Wieman, C.E.; Cornell, E.A. Vortices in a Bose–Einstein condensate. *Phys. Rev. Lett.* **1999**, *83*, 2498. [CrossRef]
3. Williams, J.E.; Holland, M.J. Preparing topological states of a Bose–Einstein condensate. *Nature* **1999**, *401*, 568–572. [CrossRef]
4. Abo-Shaeer, J.R.; Raman, C.; Vogels, J.M.; Ketterle, W. Observation of vortex lattices in Bose–Einstein condensates. *Science* **2001**, *292*, 476–479. . [CrossRef] [PubMed]
5. Madison, K.W.; Chevy, F.; Wohlleben, W.; Dalibard, J. Vortex formation in a Stirred Bose–Einstein condensate. *Phys. Rev. Lett.* **2000**, *84*, 806. [CrossRef] [PubMed]
6. Raman, C.; Abo-Shaeer, J.R.; Vogels, J.M.; Xu, K.; Ketterle W. Vortex nucleation in a stirred Bose–Einstein. condensate. *Phys. Rev. Lett.* **2001**, *87*, 210402. [CrossRef] [PubMed]
7. Cooper, N.R.; Wilkin, N.K.; Gunn, J.M.F. Quantum phases of vortices in rotating Bose–Einstein condensates. *Phys. Rev. Lett.* **2001**, *87*, 120405. [CrossRef] [PubMed]
8. Cooper, N.R. Rapidly rotating atomic gases. *Adv. Phys.* **2008**, *57*, 539–616. [CrossRef]
9. Fetter, A.L. Rotating trapped Bose–Einstein condensates. *Rev. Mod. Phys.* **2009**, *81*, 647. [CrossRef]
10. Feder, D.L.; Clark, C.W.; Schneider B.I. Nucleationn of vortex arrays in rotating anisotropic Bose–Einstein condensates. *Phys. Rev. A* **1999**, *61*, 011601. [CrossRef]
11. Jaksch, D.; Bruder, C.; Cirac, J.I.; Gardiner, C.W.; Zoller, P. Cold Bosonic Atoms in Optical Lattices. *Phys. Rev. Lett.* **1998**, *81*, 3108. [CrossRef]
12. Zhang, J.; Zhai, H. Vortex lattices in planar Bose–Einstein condensates with dipolar interactions. *Phys. Rev. Lett.* **2005**, *95*, 200403. [CrossRef] [PubMed]
13. Zhao, Y.; An, J.; Gong, C.D. Vortex competition in a rotating two-component dipolar Bose–Einstein condensate. *Phys. Rev. A* **2013**, *87*, 013605. [CrossRef]
14. Zhang, X.F.; Han, W.; Wen, L.; Zhang, P.; Dong, R.F.; Chang, H.; Zhang, S.G. Two-component dipolar Bose–Einstein condensate in concentrically coupled annular traps. *Sci. Rep.* **2014**, *10*, 08684. [CrossRef] [PubMed]
15. Sinha, S.; Castin, Y. Dynamic instability of a rotating Bose–Einstein condensate. *Phys. Rev. Lett.* **2001**, *87*, 190402. [CrossRef] [PubMed]
16. Ji, A.C.; Liu, W.M.; Song, J.L.; Zhou, F. Dynamical creation of fractionalized vortices and vortex lattices. *Phys. Rev. Lett.* **2008**, *101*, 010402. [CrossRef] [PubMed]
17. Jackson, B.; McCann, J.F.; Adams, C.S.B. Dissipation and vortex creation in Bose–Einstein condensed gases. *Phys. Rev. A* **2000**, *61*, 051603. [CrossRef]
18. Yang, T.; Xiong, B.; Benedict, K.A. Dynamical excitations in the collision of two-dimensional Bose–Einstein condensates. *Phys. Rev. A* **2013**, *87*, 023603. [CrossRef]
19. Caradoc-Davies, B.M.; Ballagh, R.J.; Burnett, K. Coherent dynamics of vortex formation in trapped Bose–Einstein Condensates. *Phys. Rev. Lett.* **1999**, *83*, 895. [CrossRef]
20. Allen, A.J.; Zaremba, E.; Barenghi, C.F.; Proukakis, N.P. Observable vortex properties in finite-temperature Bose gases. *Phys. Rev. A* **2013**, *87*, 013630. [CrossRef]
21. Jackson, B.; Proukakis, N.P.; Barenghi, C.F.; Zaremba, E. Finite-temperature vortex dynamics in Bose–Einstein condensates. *Phys. Rev. A* **2009**, *79*, 053615. [CrossRef]
22. Wright, T.M.; Bradley, A.S.; Ballagh, R.J. Finite-temperature dynamics of a single vortex in a Bose–Einstein condensate: Equilibrium precession and rotational symmetry breaking. *Phys. Rev. A* **2009**, *80*, 053624. [CrossRef]
23. Rooney, S.J.; Bradley, A.S.; Blakie, P.B. Decay of a quantum vortex: test of nonequilibrium theories for warm Bose–Einstein condensates. *Phys. Rev. A* **2010**, *81*, 023630. [CrossRef]
24. Yan, D.; Carretero-Gonzalez, R.; Frantzeskakis, D.J.; Kevrekidis, P.G.; Proukakis, N.P.; Spirn, D. Exploring vortex dynamics in the presence of dissipation: Analytical and numerical results. *Phys. Rev. A* **2014**, *89*, 043613. [CrossRef]
25. Mueller, E.J.; Ho, T.L. Two-Component Bose–Einstein condensates with a large number of vortices. *Phys. Rev. Lett.* **2002**, *88*, 180403. [CrossRef] [PubMed]
26. Kasamatsu, K.; Tsubota, M.; Ueda, M. Vortices in multicomponent Bose–Einstein condensates. *Int. J. Mod. B* **2005**, *19*, 1835. [CrossRef]
27. Lovegrove, J.; Borgh, M.O.; Ruostekoski, J. Energetically stable singular vortex cores in an atomic spin-1 Bose–Einstein condensate. *Phys. Rev. A* **2012**, *86*, 013613. [CrossRef]

28. Oh, Y.T.; Kim, P.; Park, J.H.; Han, J.H. Manifold mixing in the temporal evolution of a spin-1 spinor Bose–Einstein condensate. *Phys. Rev. Lett.* **2014**, *112*, 160402. [CrossRef] [PubMed]
29. Leanhardt, A.E.; Shin, Y.; Kielpinsk, D.I.; Pritchard, D.E.; Ketterle, W. Coreless vortex formation in a spinor Bose–Einstein condensate. *Phys. Rev. Lett.* **2003**, *90*, 140403. [CrossRef] [PubMed]
30. Koplik, J.; Levine, H. Scattering of superfluid vortex rings. *Phys. Rev. Lett.* **1996**, *76*, 4745. [CrossRef] [PubMed]
31. Caradoc-Davies, B.M.; Ballagh, R.J.; Blakie, P.B. Three-dimensional vortex dynamics in Bose–Einstein condensates. *Phys. Rev. A* **2000**, *62*, 011602. [CrossRef]
32. Kobayashi, M.; Kawaguchi, Y.; Nitta, M.; Ueda, M. Collision dynamics and rung formation of non-Abelian vortices. *Phys. Rev. Lett.* **2009**, *103*, 115301. [CrossRef] [PubMed]
33. Kaneda, T.; Saito, H. Collision dynamics of skyrmions in a two-component Bose–Einstein condensate. *Phys. Rev. A* **2016**, *93*, 033611. [CrossRef]
34. Borgh, M.O.; Ruostekoski, J. Core structure and non-Abelian reconnection of defects in a biaxial nematic spin-2 Bose–Einstein condensate. *Phys. Rev. Lett.* **2017**, *117*, 275302. [CrossRef] [PubMed]
35. Kleckner, D.; Irvine, W.T.M. Creation and dynamics of knotted vortices. *Nat. Phys.* **2013**, *9*, 253–258. [CrossRef]
36. Kleckner, D.; Kauffman, L.H.; Irvine, W.T.M. How superfluid vortex knots untie. *Nat. Phys.* **2016**, *12*, 650–655. [CrossRef]
37. Hall, D.S.; Ray, M.W.; Tiurev, K.; Ruokokosk, E.I.; Gheorghe, A.H.; Mottonen, M. Tying quantum knots. *Nat. Phys.* **2016**, *12*, 478–483. [CrossRef]
38. Freilich, D.V.; Bianchi, D.M.; Kaufman, A.M.; Langin, T.K.; Hall, D.S. Real-Time dynamics of single vortex lines and vortex dipoles in a Bose–Einstein condensate. *Science* **2010**, *329*, 1182–1185. . [CrossRef] [PubMed]
39. Neely, T.W.; Samson, E.C.; Bradley, A.S.; Davis, M.J.; Anderson, B.P. Observation of vortex dipoles in an oblate Bose–Einstein condensate. *Phys. Rev. Lett.* **2014**, *104*, 160401. [CrossRef] [PubMed]
40. Kadokura, T.; Yoshida, J.; Saito, H. Hysteresis in quantized vortex shedding. *Phys. Rev. A* **2014**, *90*, 013612. [CrossRef]
41. Kwon, W.J.; Moon, G.; Seo, S.W.; Shin, Y. Critical velocity for vortex shedding in a Bose–Einstein condensate. *Phys. Rev. A* **2015**, *91*, 053615. [CrossRef]
42. Kwon, W.J.; Seo, S.W.; Shin, Y.I. Periodic shedding of vortex dipoles from a moving penetrable obstacle in a Bose–Einstein condensate. *Phys. Rev. A* **2015**, *92*, 033613. [CrossRef]
43. Kwon, W.J.; Kim, J.H.; Seo, S.W.; Shin Y. Observation of von karman vortex street in an atomic superfluid gas. *Phys. Rev. Lett.* **2016**, *117*, 245301. [CrossRef] [PubMed]
44. Seo, S.W.; Kwon, W.J.; Kang, S.; Shin, Y. Collisional dynamics of half-quantum vortices in a spinor Bose–Einstein condensate. *Phys. Rev. Lett.* **2016**, *116*, 185301. [CrossRef] [PubMed]
45. Law, K.J.H.; Neely, T.W.; Kevrekidis, P.G.; Anderson, B.P.; Bradley, A.S.; Carretero-Gonzalez, R. Dynamic and energetic stabilization of persistent currents in Bose–Einstein condensates. *Phys. Rev. A* **2014**, *89*, 053606. [CrossRef]
46. Fujimoto, K.; Tsubota, M. Nonlinear dynamics in a trapped atomic Bose–Einstein condensate induced by an oscillating Gaussian potential. *Phys. Rev. A* **2011**, *83*, 053609. [CrossRef]
47. Gautam, S.; Roy, A.; Mukerjee, S. Finite-temperature dynamics of vortices in Bose–Einstein condensates. *Phys. Rev. A* **2014**, *89*, 013612. [CrossRef]
48. Kato, M.; Zhang, X.F.; Saito, H. Moving obstacle potential in a spin-orbit-coupled Bose–Einstein condensate. *Phys. Rev. A* **2017**, *96*, 033613. [CrossRef]
49. Aioi, T.; Kadokura, T.; Kishimoto, T.; Saito, H. Controlled generation and manipulation of vortex dipoles in a Bose–Einstein condensate. *Phys. Rev. X* **2011**, *1*, 021003. [CrossRef]
50. Gertjerenken, B.; Kevrekidis, P.G.; Carretero-Gonzalez, R.; Anderson, B.P. Generating and manipulating quantized vortices on-demand in a Bose–Einstein condensate: A numerical study. *Phys. Rev. A* **2016**, *93*, 023604. [CrossRef]
51. Samson, E.C.; Wilson, K.E.; Newman, Z.L.; Anderson, B.P. Deterministic creation, pinning, and manipulation of quantized vortices in a Bose–Einstein condensate. *Phys. Rev. A* **2016**, *93*, 023603. [CrossRef]
52. Ramanathan, A.; Wright, K.C.; Muni, S.R.Z.; Zelan, M.; Hill, W.T.; Lobb, C.; Helmerson, K.; Phillips, W.D.; Campbell, G.K. Superflow in a toroidal Bose–Einstein condensate: An atom circuit with a tunableWeak link. *Phys. Rev. Lett.* **2011**, *106*, 130401. [CrossRef] [PubMed]

53. Wright, K.C.; Blakestad, R.B.; Lobb, C.J.; Phillips, W.D.; Campbell, G.K. Driving phase slips in a superfluid atom circuit with a rotating weak link. *Phys. Rev. Lett.* **2013**, *110*, 025302. [CrossRef] [PubMed]
54. Wright, K.C.; Blakestad, R.B.; Lobb, C.J.; Phillips, W.D.; Campbell, G.K. Threshold for creating excitations in a stirred superfluid ring. *Phys. Rev. A* **2013**, *88*, 063633. [CrossRef]
55. Jendrzejewski, F.; Eckel, S.; Murray, N.; Lanier, C.; Edwards, M.; Lobb, C.J.; Campbell, G.K. Resistive flow in a weakly interacting Bose–Einstein condensate. *Phys. Rev. Lett.* **2014**, *113*, 045305. [CrossRef] [PubMed]
56. Yakimenko, A.I.; Isaieva, K.O.; Vilchinskii, S.I.; Ostrovskaya, E.A. Vortex excitation in a stirred toroidal Bose–Einstein condensate. *Phys. Rev. A* **2015**, *91*, 023607. [CrossRef]
57. Yakimenko, A.I.; Bidasyuk, Y.M.; Weyrauch, M.; Kuriatnikov, Y.I.; Vilchinskii, S.I. Vortices in a toroidal Bose–Einstein condensate with a rotating weak link. *Phys. Rev. A* **2015**, *91*, 033607. [CrossRef]
58. Eckel, S.; Jendrzejewski, F.; Kumar, A.; Lobb, C.J.; Campbell, G.K. Interferometric measurement of the current-phase relationship of a superfluid weak link. *Phys. Rev. X* **2014**, *4*, 031052. [CrossRef]
59. Abad, M. Persistent currents in coherently coupled Bose–Einstein condensates in a ring trap. *Phys. Rev. A* **2016**, *93*, 033603. [CrossRef]
60. White, A.C.; Zhang, Y.P.; Busch, T. Odd-petal-number states and persistent flows in spin-orbit-coupled Bose–Einstein condensates. *Phys. Rev. A* **2017**, *95*, 041604(R). [CrossRef]
61. Desbuquois, R.; Chomaz, L.; Yefsah, T.; Leonard, J.; Beugnon, J.; Weitenberg, C.; Dalibard, J. Superfluid behaviour of a two-dimensional Bose gas. *Nat. Phys.* **2012**, *10*, 645–648. [CrossRef]
62. Singh, V.P.; Weitenberg, C.; Dalibard, J.; Mathey L. Superfluidity and relaxation dynamics of a laser-stirred two-dimensional Bose gas. *Phys. Rev. A* **2017**, *95*, 043631. [CrossRef]
63. Choi, S.; Morgan, S.A.; Burnett, K. Phenomenological damping in trapped atomic Bose–Einstein condensates. *Phys. Rev. A* **1998**, *57*, 4057. [CrossRef]
64. Castin, Y. Simple theoretical tools for low dimension Bose gases. *J. Phys. IV (France)* **2004**, *116*, 89. [CrossRef]
65. Inouye, S.; Gupta, S.; Rosenband, T.; Chikkatur, A.P.; Gorlitz, A.; Gustavson, T.L.; Leanhardt, A.E.; Pritchard, D.E.; Ketterle, W. Observation of vrtex phase singularities in Bose–Einstein condensates. *Phys. Rev. Lett.* **2001**, *87*, 080402. [CrossRef] [PubMed]
66. Landau, L.D.; Lifshitz, E.M. *Fluid Mechanics*; Pergamon Press: Oxford, UK, 1987.
67. Onofrio, R.; Durfee, D.S.; Raman, C.; Kohl, M.; Kuklewicz, C.; Ketterle, W. Surface excitations of a Bose–Einstein condensate. *Phys. Rev. Lett.* **2000**, *84*, 810. [CrossRef] [PubMed]
68. Dalfovo, F.; Stringari, S. Shape deformations and angular-momentum transfer in trapped Bose–Einstein condensates. *Phys. Rev. A* **2000**, *63*, 011601(R). [CrossRef]
69. Recati, A.; Zambelli, F.; Stringari, S. Overcritical rotation of a trapped Bose–Einstein Condensate. *Phys. Rev. Lett.* **2001**, *86*, 377. [CrossRef] [PubMed]
70. Stringari, S. Collective Excitations of a Trapped Bose-Condensed Gas. *Phys. Rev. Lett.* **1996**, *77*, 2360. [CrossRef] [PubMed]
71. Pinsker, F.; Berloff, N.G. Transitions and excitations in a superfluid stream passing small impurities. *Phys. Rev. A* **2014**, *89*, 053605. [CrossRef]
72. Winiecki, T.; McCann, J.F.; Adamas, C.S. Pressure dDrag in linear and nonlinear quantum fluids. *Phys. Rev. Lett.* **1999**, *82*, 5186. [CrossRef]